



WFIRST Coronagraph Instrument Reference Information

September 2018

Information here captures the instrument design as of
CGI System Requirements Review in May 2018.

John Trauger

on behalf of the WFIRST-CGI Science and Engineering Project
Jet Propulsion Laboratory, California Institute of Technology

Coronagraph Instrument (CGI)

The Coronagraph Instrument on WFIRST is an advanced technology demonstrator for future missions aiming to directly image Earth-like exoplanets.

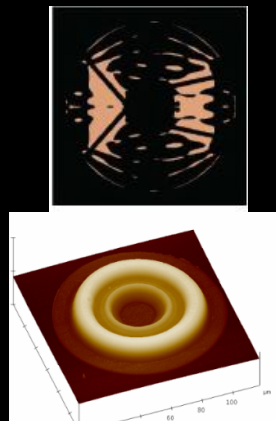
Autonomous Ultra-Precise Wavefront Sensing & Control



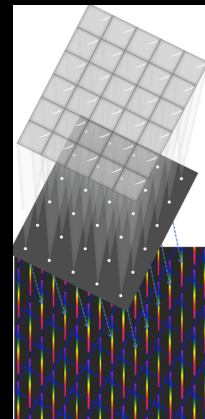
Large-format Deformable Mirrors



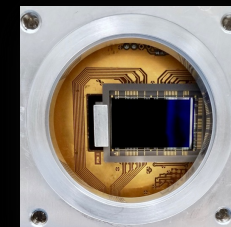
High-contrast Coronagraph Masks



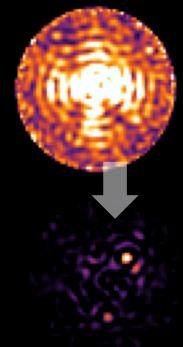
High-contrast Integral Field Spectroscopy



Ultra-low noise photon counting Visible Detectors

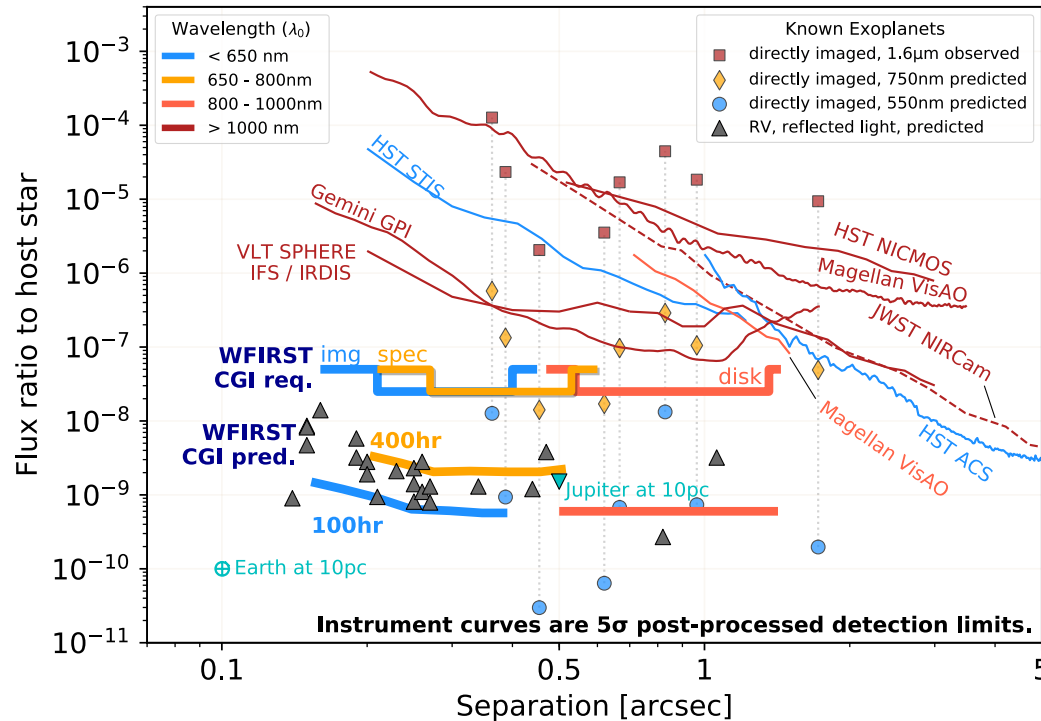


Data Post-Processing



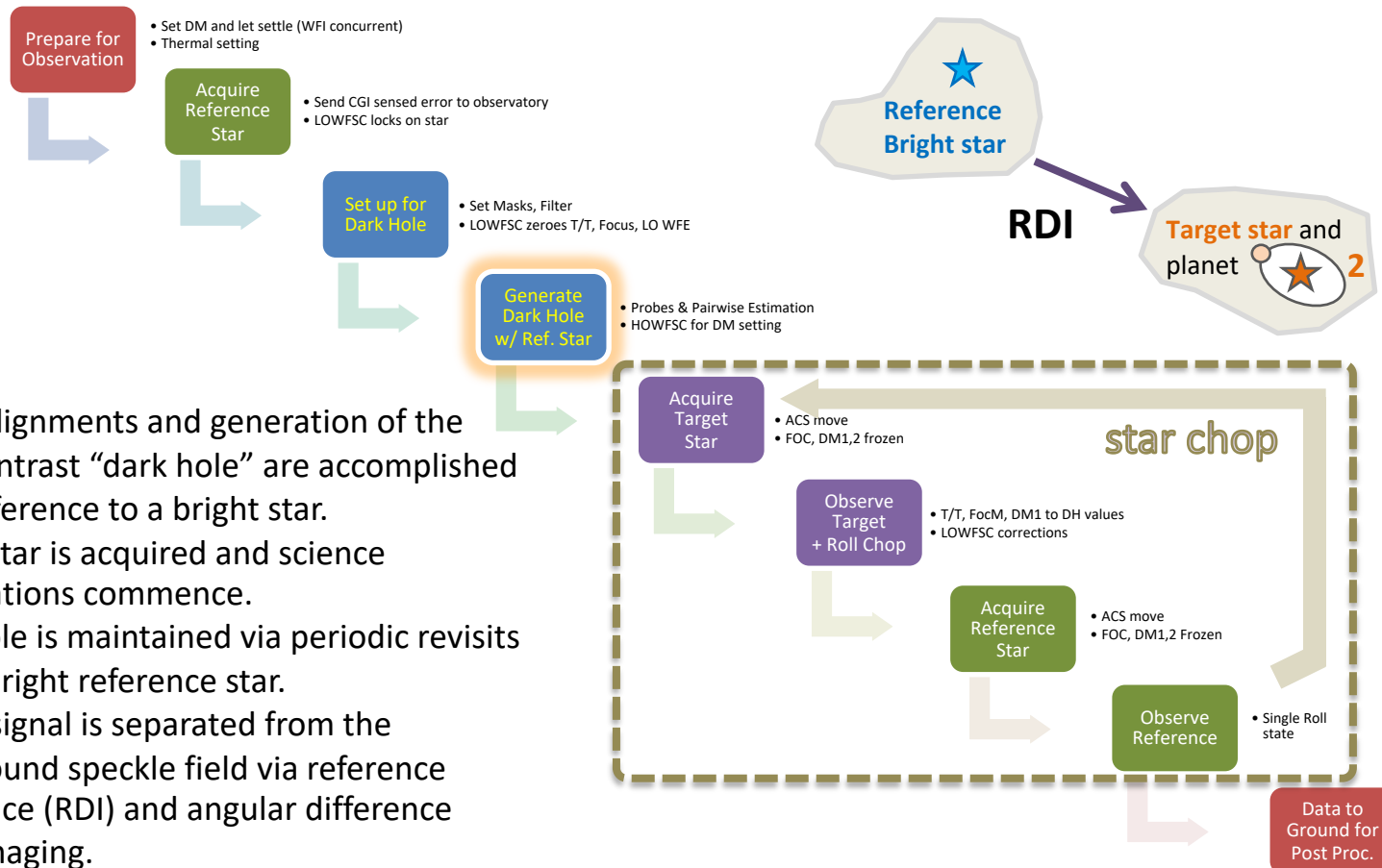
CGI will premiere in space the technologies needed to image and characterize rocky planets in the habitable zones of nearby stars. By demonstrating these tools in a system with end-to-end, scientific observing operations, NASA will reduce the cost and risk of a potential future flagship mission.

Required & Predicted CGI Performance in the Context of Existing Astronomy Capabilities



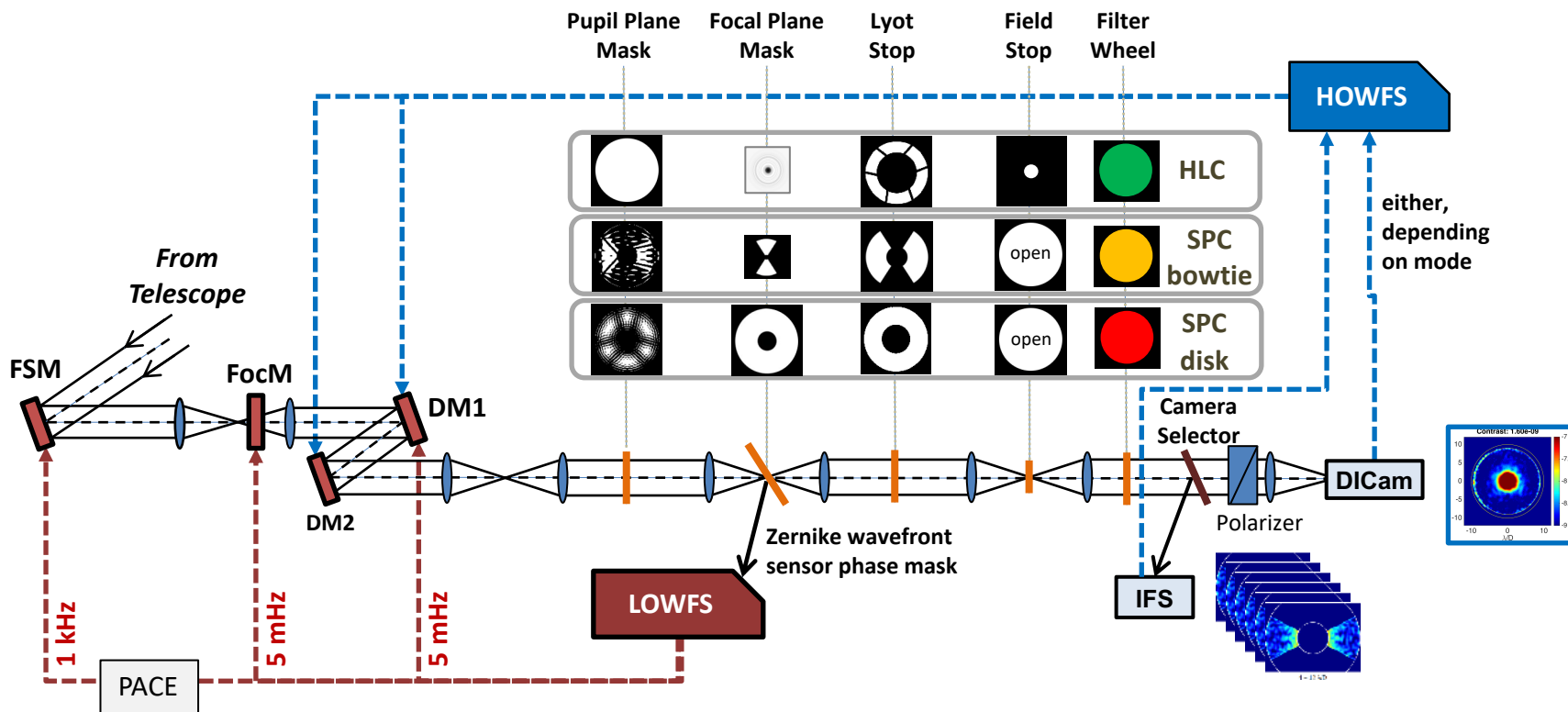
Instrument performance requirements and current-best-estimated performance are based on laboratory demonstrations and model predictions, as of the CGI System Requirements Review in May 2018. Laboratory demonstrations and model refinements are ongoing in Phase B development. See V. Bailey, <https://caltech.app.box.com/v/nas-cgi/file/282502834046> for a detailed description of this plot.

Operations Concept: autonomous steps



- Initial alignments and generation of the high-contrast “dark hole” are accomplished with reference to a bright star.
- Target star is acquired and science observations commence.
- Dark hole is maintained via periodic revisits of the bright reference star.
- Planet signal is separated from the background speckle field via reference difference (RDI) and angular difference (ADI) imaging.
- Routine observing sequences are carried out autonomously.

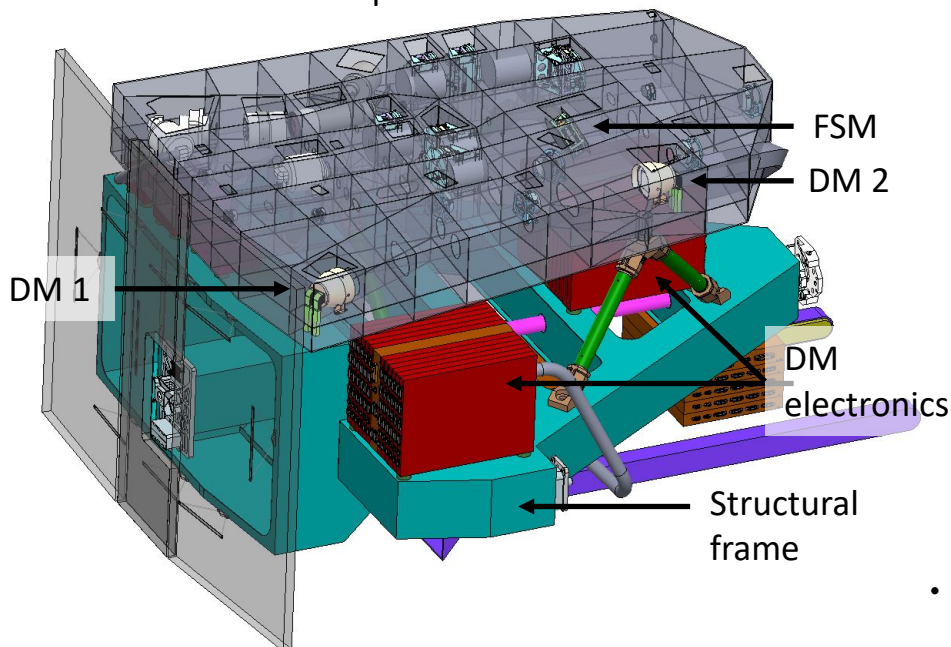
CGI Architecture



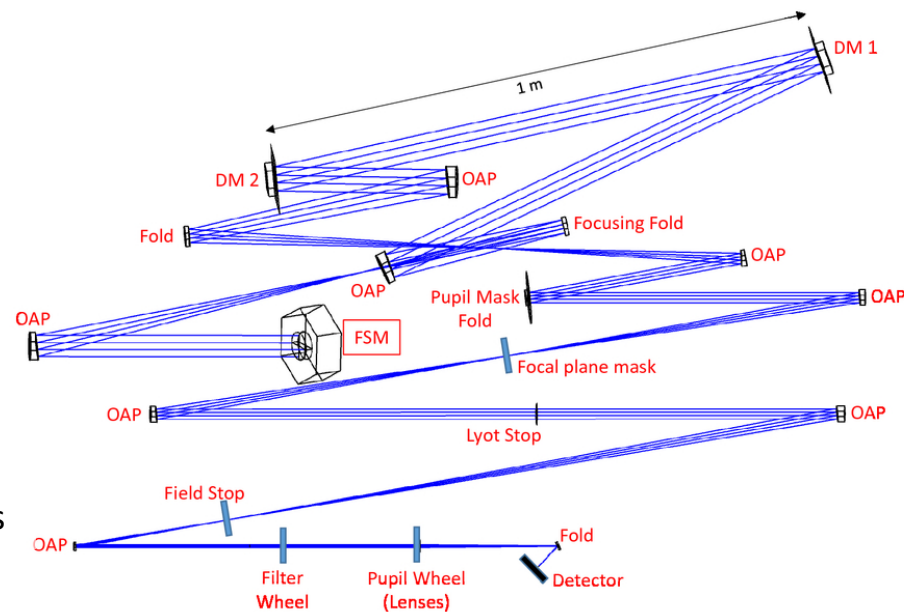
- Two selectable coronagraph technologies (HLC, SPC)
- Two deformable mirrors (DMs) for high-order wavefront control
- Low-order wavefront sensing & control (LOWFS&C)
- Direct imaging camera (DICam)
- Integral field spectrograph (IFS, R = 50)
- Photon-counting EMCCD detectors

CGI Architecture

CGI optical bench

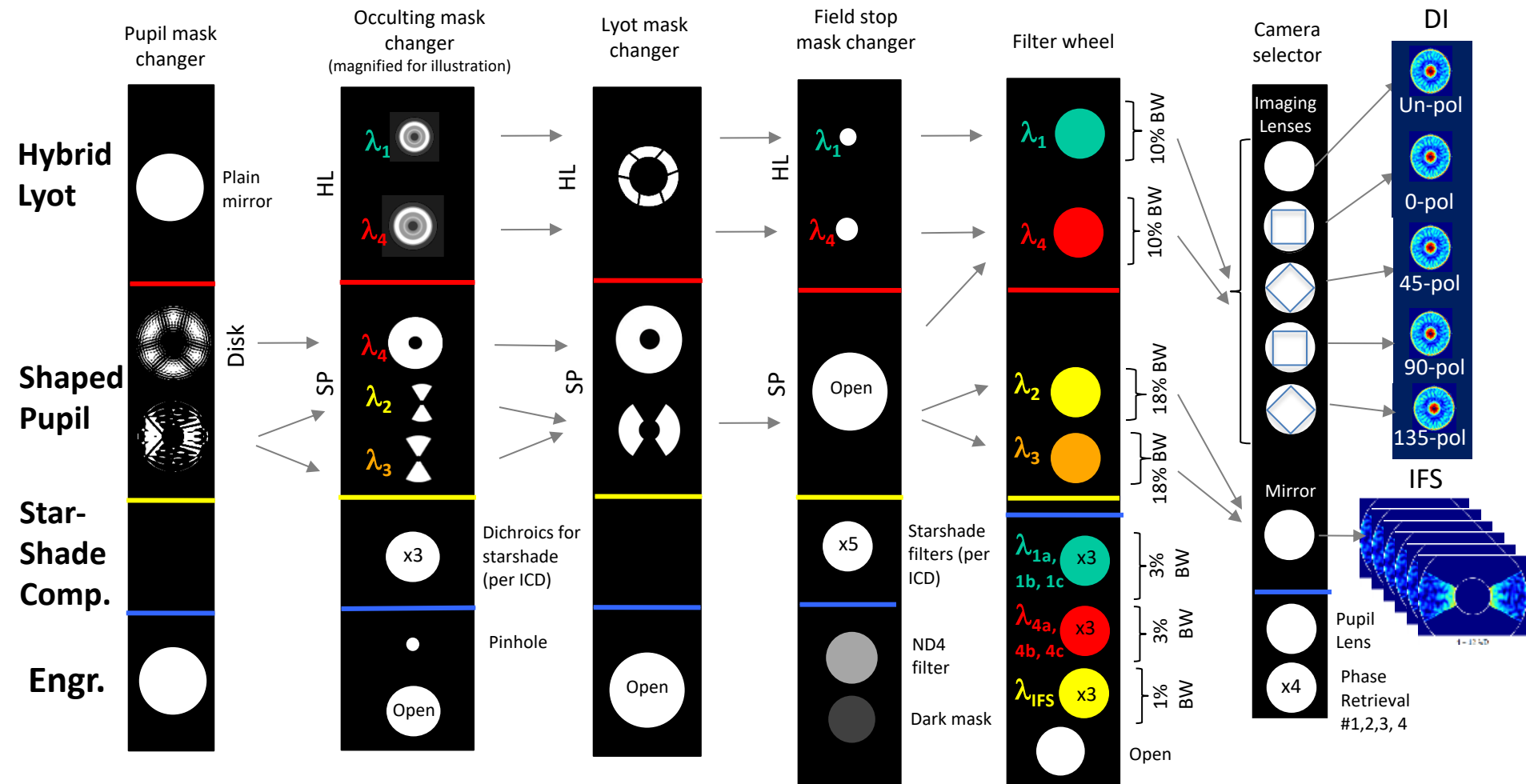


- In the WFIRST Payload, CGI mounts onto the Instrument Carrier (IC) shared with the Wide Field Instrument. The Tertiary Collimator Assembly (TCA; not shown) is the optical interface between the telescope and CGI, and relays an exit pupil onto the Fast Steering Mirror (FSM).
- Phase A design as of May 2018.



- The first deformable mirror, **DM 1**, is positioned at a relay pupil following the **FSM**. **DM 2** is positioned 1 meter away to enable correction of amplitude errors and phase errors originating from out-of-pupil surfaces.
- Both coronagraph mask types, the Hybrid Lyot and Shaped Pupil Coronagraphs (HLC and SPC), are implemented on the same optical beam train and selected by changing masks at the planes labeled **Pupil Mask Fold**, **Focal plane mask**, and **Lyot Stop**.
- The filter and the camera channel (either the Direct Imaging Camera or the Integral Field Spectrograph) are selected by mechanisms after the Lyot stop.

Coronagraph Elements



$\lambda_1=575 \text{ nm, } 10\%$ $\lambda_2=660 \text{ nm, } 18\%$ $\lambda_3=760 \text{ nm, } 18\%$ $\lambda_4=825 \text{ nm, } 10\%$

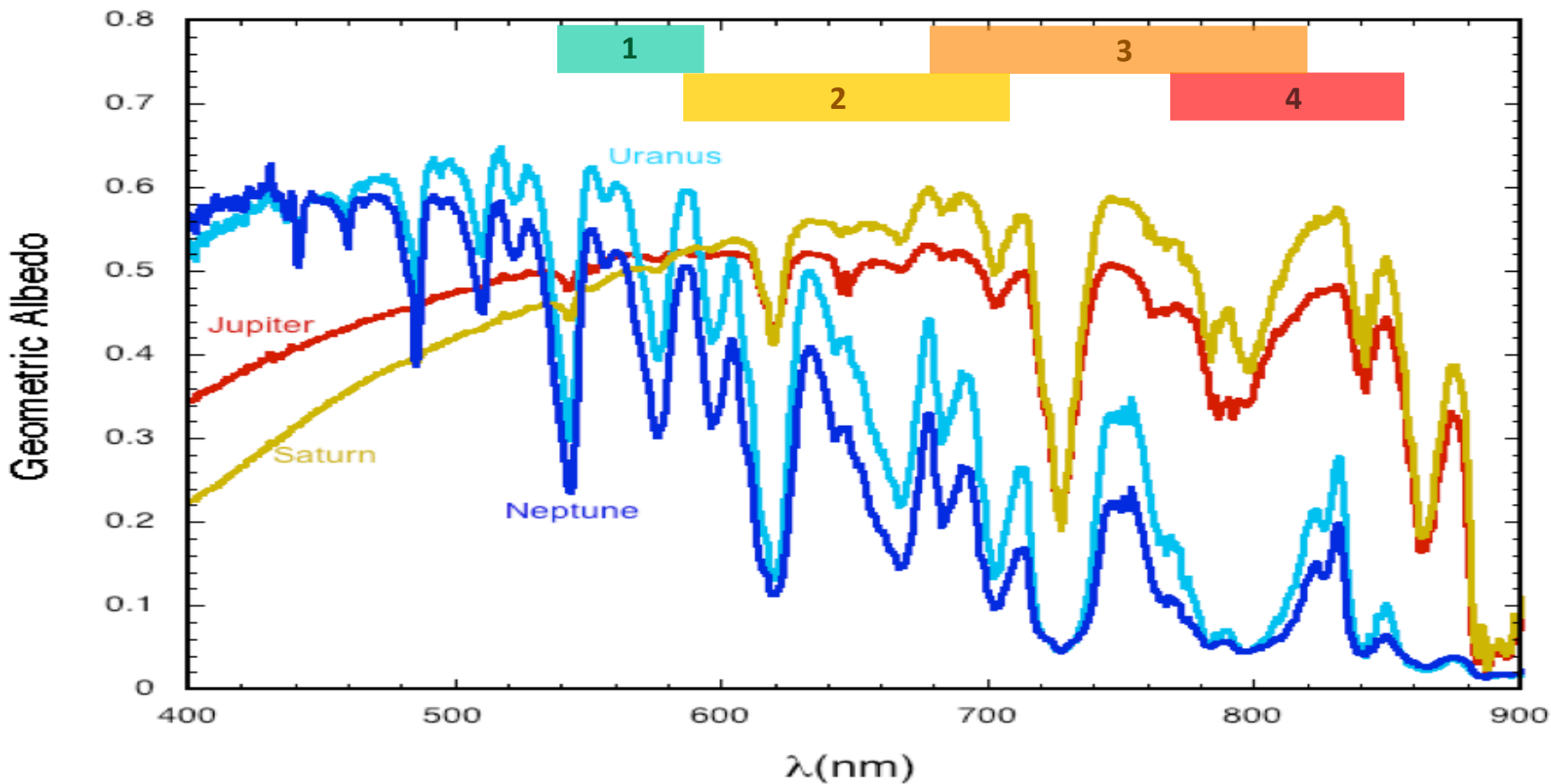


WFIRST
 WIDE-FIELD INFRARED SURVEY TELESCOPE
 DARK ENERGY • EXOPLANETS • ASTROPHYSICS



Baseline Science Filters

$\lambda_1=575$ nm, 10% $\lambda_2=660$ nm, 18% $\lambda_3=760$ nm, 18% $\lambda_4=825$ nm, 10%





WFIRST
 WIDE-FIELD INFRARED SURVEY TELESCOPE
 DARK ENERGY • EXOPLANETS • ASTROPHYSICS



CGI Observing Modes



CGI Filter	λ_{center} (nm)	BW	Channel	Mask Type	Working Angle	Can use w/ linear polarizers	Starlight Suppression Region
1	575	10%	Imager	HLC	3-9 λ/D	Y	360°
3	760	18%	IFS	SPC bowtie	3-9 λ/D		130°
4	825	10%	Imager	SPC wide FOV	6.5-20 λ/D	Y	360°

These three “official” modes will be fully tested prior to launch and will be utilized during the formal tech demonstration. Flight hardware is configurable with other filter and coronagraph combinations that will be characterized on engineering testbeds, but will not be fully tested prior to launch.

$\lambda_1=575$ nm, 10% $\lambda_2=660$ nm, 18% $\lambda_3=760$ nm, 18% $\lambda_4=825$ nm, 10%

CGI Configurations

CGI Filter	λ_{center} (nm)	BW	Mask Type	Working Angle	Starlight Suppression Region
1	575	10%	HLC	3-9 λ/D	360°
2	660	18%	SPC bowtie	3-9 λ/D	130°
3	760	18%	SPC bowtie	3-9 λ/D	130°
4	825	10%	SPC wide FOV	6.5-20 λ/D	360°
4	825	10%	HLC	3-9 λ/D	360°

These five coronagraph masks will be installed in CGI. However, only the three CGI configurations supporting the “official observing modes” will be fully tested for the tech demo phase.

$\lambda_1=575$ nm, 10% $\lambda_2=660$ nm, 18% $\lambda_3=760$ nm, 18% $\lambda_4=825$ nm, 10%



WFIRST
WIDE-FIELD INFRARED SURVEY TELESCOPE
DARK ENERGY • EXOPLANETS • ASTROPHYSICS

Starshade Compatibility

Starshade filters

λ (nm)	BW	$\Delta\lambda$	λ_{\min} (nm)	λ_{\max} (nm)	mode
488.5	26.0%	127	425	552	img
707.5	26.1%	185	615	800	img
728	19.8%	144	656	800	IFS
884.5	26.1%	231	769	1000	img
910	19.8%	180	820	1000	IFS

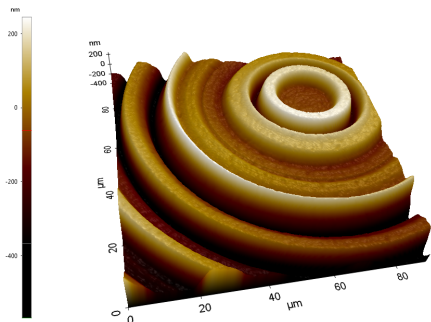
These filters accommodate observations with a potential future starshade probe mission. They are held in the CGI Field Stop changer (column 4 of the mask-filter schematic in slide 6).

Starshade probe concept study reports available at
<https://exoplanets.nasa.gov/exep/studies/probe-scale-stdt/>

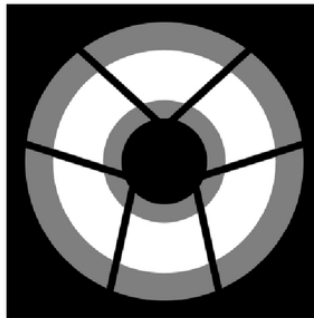
- The WFIRST baseline design is starshade-ready, to support exoplanet observations with an external starshade occulter in the event that one is launched in the future.
- CGI has 3 starshade-dedicated dichroic Zernike sensor masks in the occulter wheel to enable lateral starshade position sensing using the LOWFS camera.
- CGI has 5 dedicated filters for scientific observations with a starshade, suitable for both the direct imaging and IFS cameras.

Hybrid Lyot Coronagraph

- The HLC provides a full 360° high contrast field of view.
- Focal plane occulting mask is a circular, $r = 2.8 \lambda_c/D$ partially-transmissive nickel disc overlaid with a dielectric layer with a radially and azimuthally varying thickness profile.
- The HLC design incorporates a numerically optimized, static actuator pattern applied to both deformable mirrors.
- Lyot stop is an annular mask that blocks the telescope pupil edges and struts.
- September 2018 updated design PSF core throughput is 5.2% relative to the energy incident on primary mirror (ignoring losses from reflections and filters).

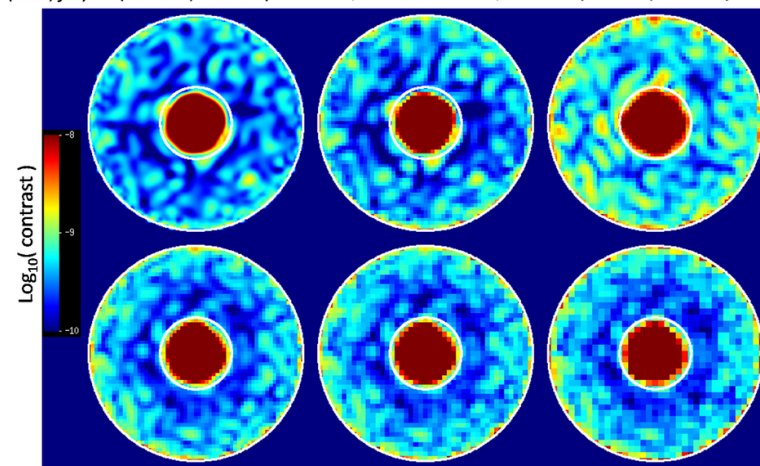


HLC occulting mask. AFM surface height measurement of an occulting mask fabricated by the JPL Micro Devices Lab. Recent design refinements include azimuthal ripples in thickness of the dielectric, which extends across the field of view.



HLC Lyot stop. Diagram of Lyot stop model: white represents the transmitted region; black represents the telescope pupil; gray represents the region blocked by the stop in addition to the telescope pupil.

9 wavelengths, perfect knowledge 0.2 λ_c/D point sampling (Inner, full) = (3.8x10 ⁻¹⁰ , 4.2x10 ⁻¹⁰)	9 x 1.1% sub-bands, probing, 0.3 λ_c/D finite pixels (4.2x10 ⁻¹⁰ , 4.6x10 ⁻¹⁰)	2 x 5% sub-bands, probing, 0.3 λ_c/D finite pixels (9.0x10 ⁻¹⁰ , 7.8x10 ⁻¹⁰)
---	--	--



3 x 3.3% sub-bands, probing, 0.3 λ_c/D finite pixels (3.3x10 ⁻¹⁰ , 5.0x10 ⁻¹⁰)	3 x 3.3% sub-bands, probing, 0.4 λ_c/D finite pixels (3.2x10 ⁻¹⁰ , 5.3x10 ⁻¹⁰)	3 x 3.3% sub-bands, probing, 0.5 λ_c/D finite pixels (3.3x10 ⁻¹⁰ , 5.5x10 ⁻¹⁰)
--	--	--

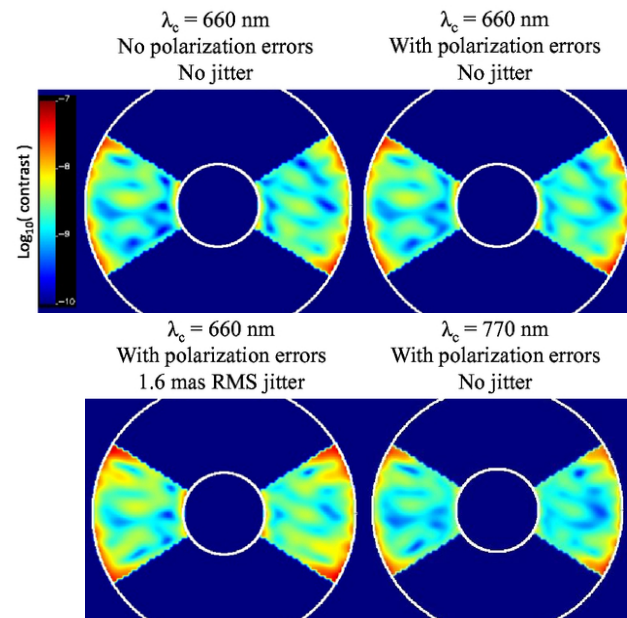
Simulated HLC PSF including aberrations and high-order wavefront control operations, illustrating the annular dark zone between 3 and 9 λ_c/D . Each sub-panel represents a different scenario for DM probe wavelength resolution and detector sampling.

References

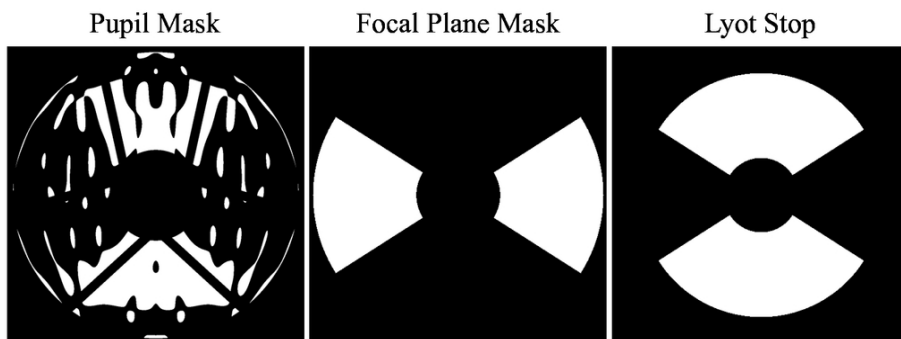
- J. Trauger, D. Moody, et al., JATIS Vol 2, id. 011013 (2016) - <https://doi.org/10.1117/1.JATIS.2.1.011013>
- J. Krist, et al., Proc SPIE Vol 10400, id. 1040004. (2017) - <http://dx.doi.org/10.1117/12.2274792>
- K. Balasubramanian, et al., Proc SPIE Vol 10400, id. (2017) - <https://doi.org/10.1117/12.2274059>

Shaped Pupil Coronagraph

- The shaped pupil apodizer is a reflective mask on a silicon substrate with aluminum regions for reflection and black silicon regions for absorption.
- The hard-edged occulting mask has either a bowtie-shaped opening for characterization (spectroscopy) mode or an annular aperture for debris disk imaging.
- The Characterization SPC designed in 2017 produces a $2 \times 65^\circ$ bowtie dark zone from $3 - 9 \lambda_c/D$ over an 18% bandpass, and has a PSF core throughput of 3.8% relative to the energy incident on primary mirror (ignoring losses from reflections and filters).
- The Debris Disk SPC design produces a 360° dark zone from $6.5 - 20 \lambda_c/D$ in a 10% bandpass.



Characterization SPC simulations at $\lambda_c = 660$ and 770 nm including system aberrations, pointing jitter, and wavefront control operations. The circles correspond to $r = 3$ and $9 \lambda_c/D$.



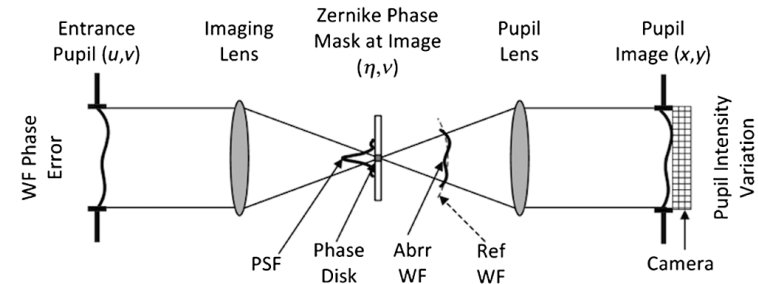
Characterization shaped pupil coronagraph masks from 2017.
Design by A. J. E. Riggs.

References

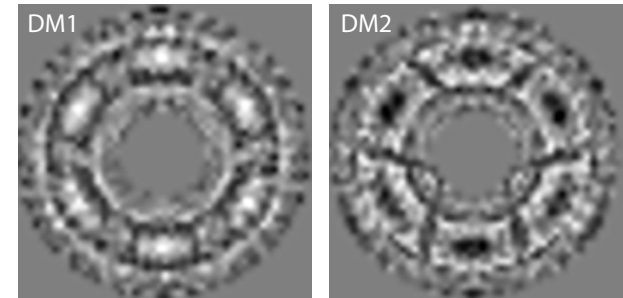
- N. T. Zimmerman, et al., JATIS Vol 2 id. 011012 (2016) - <http://dx.doi.org/10.1117/1.JATIS.2.1.011012>
- K. Balasubramanian, et al., JATIS Vol2 id. 011005 (2015) - <https://doi.org/10.1117/1.JATIS.2.1.011005>
- A. J. E. Riggs et al., N. T. Zimmerman, et al., Proc SPIE Vol 10400 (2017) - <http://dx.doi.org/10.1117/12.2274437>
- J. Krist, et al., Proc SPIE Vol 10400, id. 1040004. (2017) - <http://dx.doi.org/10.1117/12.2274792>

Wavefront Control

- The baseline CGI design includes four active optics to control the wavefront: a **fast steering mirror** (FSM), a flat **focusing mirror** (FocM), and two **deformable mirrors** (DM 1 and DM 2) with 48x48 actuators each.
- High-order wavefront control is implemented by the Electric Field Conjugation (EFC) method. The EFC loop operates on science focal plane data by measuring the interaction of aberrated on-axis starlight with a sequence of DM actuator probes.
- Pointing, focus, and low-order wavefront drifts are sensed by the **Low-Order Wavefront Sensing and Control** (LOWFS/C) subsystem using the Zernike phase-contrast technique on starlight rejected from the occulting mask. Corrections to Zernike modes Z5—Z11 are applied to DM 1.
- The FSM control loop corrects line-of-sight pointing jitter to below 0.8 milliarcsec.



Conceptual diagram of the Zernike phase contrast wavefront sensor (F. Shi, et al., 2016).



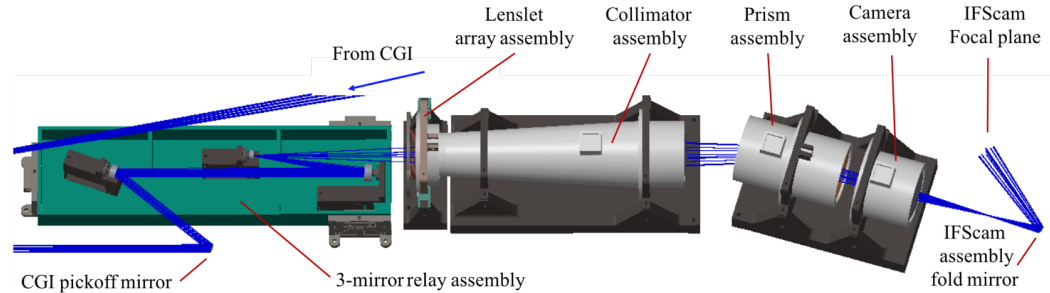
Optimized DM surfaces applied in HLC data simulations.

References

- T. Groff, A. J. E. Riggs, et al., JATIS Vol 2, id 011009 (2015) - <https://doi.org/10.1117/1.JATIS.2.1.011009>
- F. Shi, et al., JATIS Vol 2, id 011021 (2016) - <https://doi.org/10.1117/1.JATIS.2.1.011021>
- J. Krist, et al., JATIS Vol 2, id 011003 (2015) - <https://doi.org/10.1117/1.JATIS.2.1.011003>

Integral Field Spectrograph

- Lenslet-based integral field spectrograph (IFS) with $R=50$ spectral resolving power and a 1.6-arcsec field of view.
- A reflective relay feeds a lenslet array, which critically samples the coronagraph image (2 lenslets per λ_c/D at 660 nm). The light from each spatial element is dispersed by a prism group.
- The prioritized spectroscopy demonstration filter is an 18% bandpass centered at 760 nm (CGI Science Band 3) matched to the characterization SPC. However, by design the IFS can capture an instantaneous bandpass up to 20% anywhere in the range 600 to 1000 nm.



Baseline opto-mechanical layout of the CGI IFS, showing the beam progression through the relay mirrors, lenslet array, collimator, prism, and reimaging optics. The spectra are focused on a dedicated EMCCD detector (the IFScam; not shown).



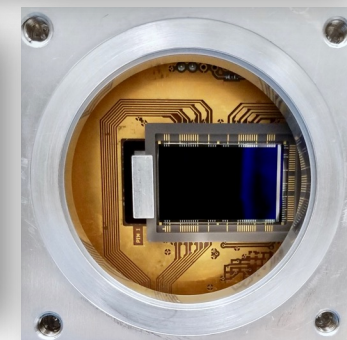
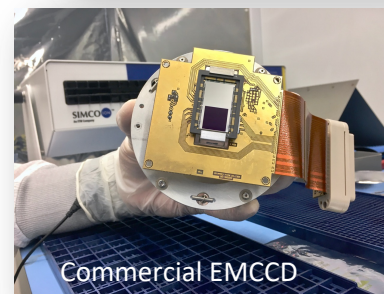
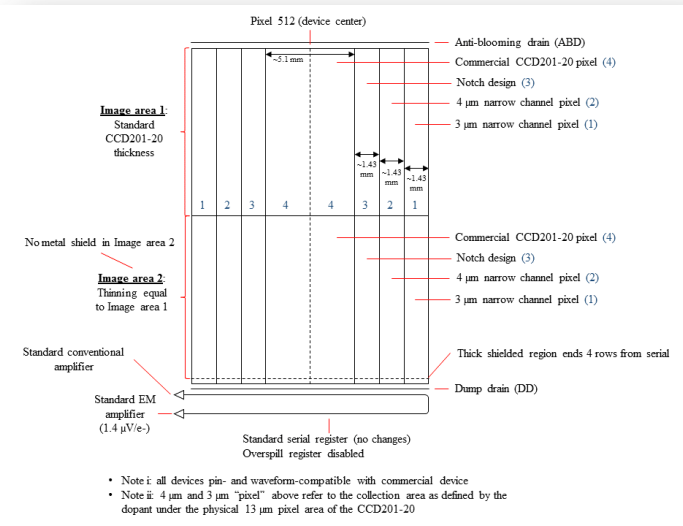
The IFS produces a spectrally dispersed map of the CGI focal plane, comprised of a grid of interleaved microspectra. There is one microspectrum for each lenslet, or spatial element (center). A wavelength-resolved data cube (right hand side) is reconstructed by software.

References

- M. McElwain, A. Mandell, Q. Gong, et al., Proc SPIE Vol 9904 (2016)
- M. Rizzo, T. Groff, N. Zimmerman, et al., Proc SPIE Vol 10400 (2017)
- A. Mandell, T. Groff, Q. Gong, et al., Proc SPIE Vol. 10400 (2017)

- Electron Multiplying CCD (EMCCD) technology is advantageous for a coronagraph application.
 - Programmable gain provides wide dynamic range suitable for bright scenes expected during acquisition and coronagraph configuration, while photon counting capability can be used for faint light observations with zero read noise.
- EMCCD detectors are baselined for direct imaging, spectroscopy and wavefront sensing applications in CGI.
 - Subarray readout suitable for a wavefront sensor application enables 1000 frame-s⁻¹ operation to accommodate tip-tilt sensing.
- Work at JPL is focused on low flux characterization with radiation damaged sensors.
 - JPL is investing in modifications to the commercial version of the EMCCD that are expected to improve margins against radiation damage in a flight environment. Characterization of flight prototype devices is planned for FY19.
- JPL's EMCCD test lab has measured a low flux threshold of 0.002 c-psf⁻¹-s⁻¹, equivalent to a 32.4 magnitude star through a 2.4m telescope at 500 nm with 10% bandwidth.
 - Devices irradiated to 5 years equivalent life at L2 meet coronagraph technology requirements. Low flux QE is reduced 20-25% and dark current is increased ~2x.

Radiation-hardened EMCCDs are in Production

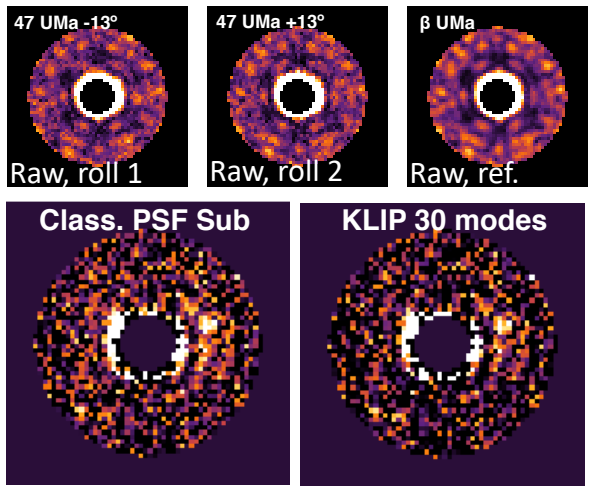


References

- [L. Harding, R. Demers, et al., JATIS Vol 2, id 011007 \(2016\)](#)

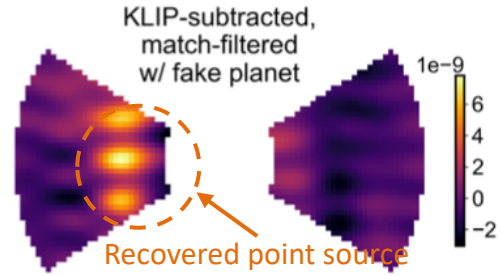
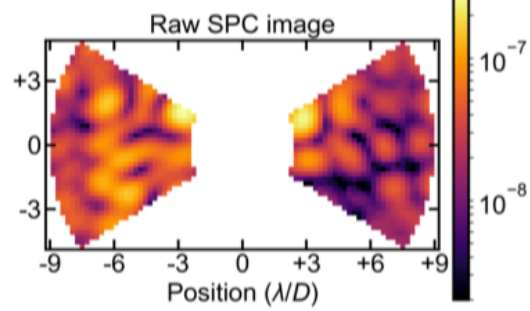
- Investigations on algorithms for CGI data post-processing have encompassed both end-to-end data simulations and analysis of laboratory testbed data.
- Reference differential imaging* (RDI) trials have probed a range of wavefront stability and noise scenarios. Simulations with spacecraft rolls have also enabled tests of *Angular differential imaging* (ADI).

1. Post-processing trials on HLC data simulations

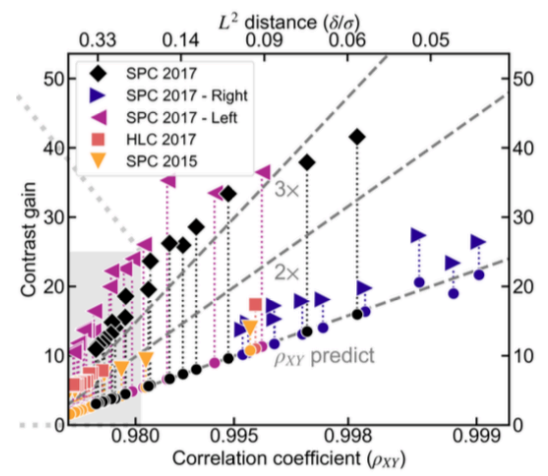


September 2018

2. Post-processing trials on Laboratory Data



Example application of RDI to SPC data from the HCIT, demonstrating the match-filtered recovery of a fake point source inserted into one image.



Post-processing contrast gain plotted against reference library correlation for five datasets. Above a certain correlation coefficient, the post-processing gain is comparable to the gain from classical PSF subtraction.

References

- N. Zimmerman, L. Pueyo, R. Soummer, B. Mennesson, JATIS submitted.
- M. Ygouf, N. Zimmerman, L. Pueyo, R. Soummer, et al., Proc. SPIE Vol 9904 (2016) - <http://dx.doi.org/10.1117/12.2231581>

- The WFIRST Exoplanet Data Challenges are a series of blind retrieval exercises based on simulated CGI data, to explore instrument capabilities, and inform design choices and operations concepts.
- Upcoming Data Challenge #2: Extracting planets from images
- Test planet discrimination from background using photometry (epoch 1), proper motion (epoch 2)
- Test orbit determination (epoch 3)
- Test enhanced detection/orbit determination capability with late-mission starshade images (epochs 4, 5)
- Opening date of challenge - late October, recruit participants through end of year including January AAS

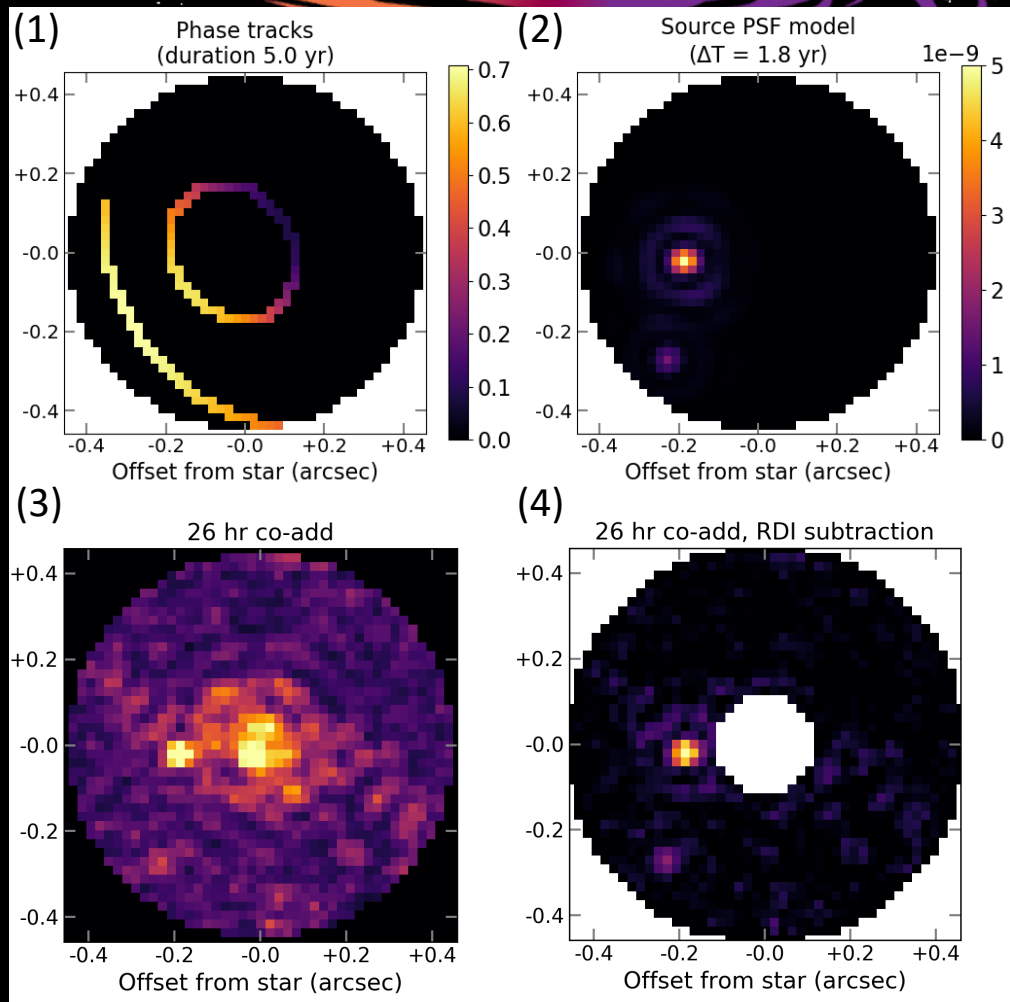
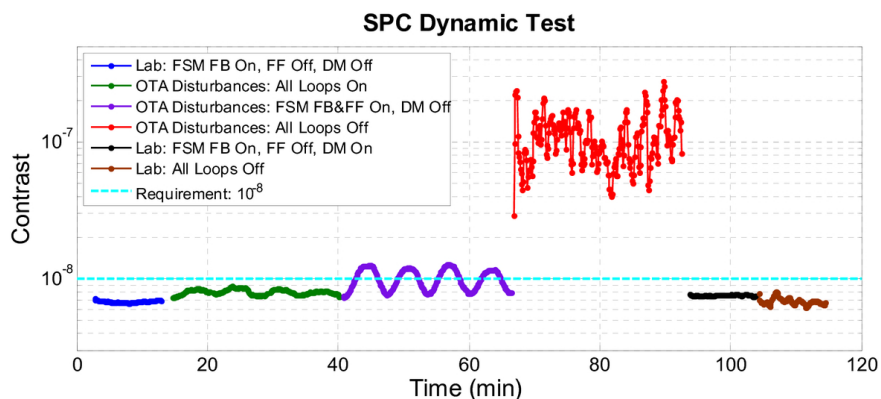
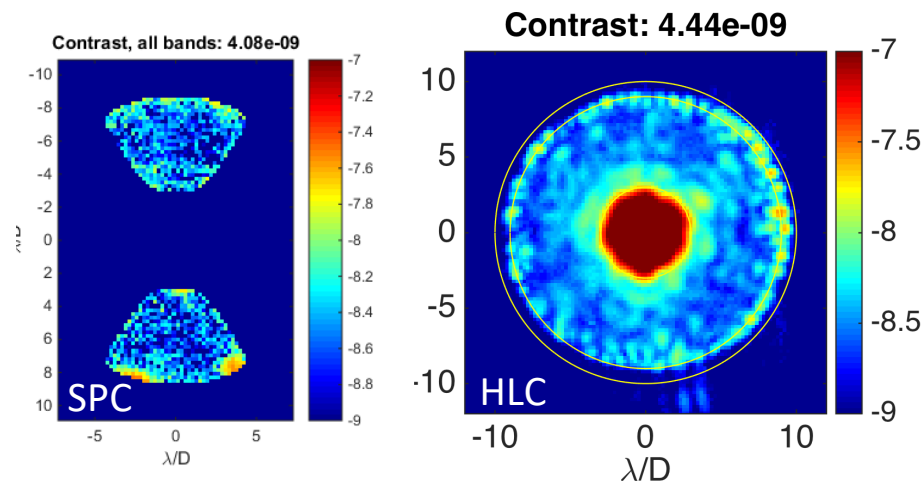


Image data challenge under preparation: (1) Model phase function tracks for a 2-planet system; (2) Source PSF model at one epoch; (3) Simulated co-add based on OS6 HLC time series; (4) Recovery of scene after RDI post-processing.

Results from the Occulting Mask Coronagraph (OMC) Testbed at JPL HCIT



Dynamic contrast demonstration with a Low Order Wavefront Sensing and Control (LOWFS/C) system integrated on the Occulting Mask Coronagraph testbed. When line-of-sight disturbances and low order wavefront drift (slow varying focus) are introduced on the testbed, the LOWFS senses the pointing error and wavefront drift and corrects them by commanding a fast steering mirror and one of the DMs. Demonstrations with both the SPC and HLC masks surpassed their $1E-8$ contrast goal (F. Shi, et al., Proc SPIE Vol 10400, 2017).



Normalized intensity maps measured on the OMC testbed in broadband (10 %) light for SPC (left) and HLC. The total contrast between $3 - 9 \lambda/D$ is listed on top of each figure.

References

- F. Shi, E. Cady, et al., Proc. SPIE Vol 10400 (2017) - <http://dx.doi.org/10.1117/12.2274887>
- E. Cady, K. Balasubramanian, et al., Proc. SPIE Vol 10400 (2017) - <http://dx.doi.org/10.1117/12.2272834>
- B.-J. Seo, E. Cady, et al., Proc SPIE Vol 10400, 10.1117/12.2274687 (2017) - <http://dx.doi.org/10.1117/12.2274687>
- F. Shi, et al., Proc. SPIE Vol 10698 (2018) - <https://doi.org/10.1117/12.2312746>
- B.-J. Seo, et al, Proc. SPIE Vol 10698 (2018) - <https://doi.org/10.1117/12.2314358>
- D. Marx, et al, Proc. SPIE Vol 10698 (2018) - <https://doi.org/10.1117/12.2312602>



WFIRST
 WIDE-FIELD INFRARED SURVEY TELESCOPE
 DARK ENERGY • EXOPLANETS • ASTROPHYSICS



Simulation Resources

Name	Author	Description	Format	URL	References
WFIRST Coronagraph Instrument (CGI) Imaging Simulations	John Krist (JPL)	Time series CGI imaging data simulations produced by JPL, incorporating observatory STOP models and wavefront control.	FITS files	https://wfirst.ipac.caltech.edu/sims/Coronagraph_public_images.html	<p>J. Krist, et al., <i>JATIS Vol 2, id. 011003 (2016)</i></p> <p>J. Krist, et al., <i>Proc SPIE Vol 10400, id. 1040004. (2017)</i></p>
EXOSIMS	Dmitry Savransky (Cornell U.)	Exoplanet Open-Source Imaging Mission Simulator, with dedicated configurations for simulating CGI surveys and integration times.	web browser interface	https://wfirst.ipac.caltech.edu/sims/tools/exosimsCGI/exosimsCGI.html	<i>D. Savransky & D. Garrett, JATIS Vol 2, id. 011006 (2016)</i>
			Python source code	https://github.com/dsavransky/EXOSIMS	<i>C. Delacroix, D. Savransky, et al., Proc SPIE Vol 9911, id. 991119 (2016)</i>
WebbPSF	Marshall Perrin (STScI)	Simulated Point Spread Functions for WFIRST WFI and CGI (static)	Python source code, with tutorials	https://github.com/mperrin/webbpsf	<p>M. Perrin, et al., <i>Proc SPIE Vol 8442, article id. 84423D (2012)</i></p> <p>M. Perrin, et al., <i>Proc SPIE Vol 9143, id. 91433X (2014)</i></p>
CRISPY	Maxime Rizzo (GSFC)	Coronagraph Rapid Imaging Spectrograph in Python - IFS simulations, tools for laboratory testbed demonstrations.	Python source code, with descriptive overview	https://wfirst.ipac.caltech.edu/sims/Crispy_simulations.html	<i>M. Rizzo, et al., Proc SPIE Vol 10400, id. 104000B (2017)</i>

Reference documents

Reference	URL	Year
<i>Wide-Field Infrared Survey Telescope-Astrophysics Focused Telescope Assets (WFIRST-AFTA) 2015 Report</i> by the Science Definition Team (SDT) and WFIRST Study Office	https://wfirst.gsfc.nasa.gov/science/sdt_public/WFIRST-AFTA_SDT_Report_150310_Final.pdf	2015
Journal of Astronomical Telescopes Instruments and Systems, Vol. 2, No. 1, <i>Special Section on WFIRST-AFTA Coronagraphs</i> , eds. Olivier Guyon and Motohide Tamura	https://www.spiedigitallibrary.org/journals/Journal-of-Astronomical-Telescopes-Instruments-and-Systems/volume-2/issue-01#Editorial	2016
SPIE Proceedings Vol. 10400, <i>Techniques and Instrumentation for Detection of Exoplanets VIII</i> , ed. Stuart Shaklan	https://www.spiedigitallibrary.org/conference-proceedings-of-spie/10400	2017
SPIE Proceedings Vol. 10698, <i>Space Telescopes and Instrumentation 2018: Optical, Infrared, and Millimeter Wave, WFIRST I, II, III</i>	https://www.spiedigitallibrary.org/conference-proceedings-of-spie/10698	2018
<i>Community White Papers submitted to the NAS Exoplanet Science Strategy Committee, co-chairs D. Charbonneau & S. Gaudi. Among the CGI-related papers are: Kasdin et al., Bailey et al., Mennesson et al., Marley et al., B. Crill et al., and others.</i>	http://sites.nationalacademies.org/SSB/CurrentProjects/SSB_180659	2018